Fluid Dynamics and Co-located Conferences
June 24-27, 2013, San Diego, CA
31st AIAA Applied Aerodynamics Conference

Transonic Tail Buffet Simulations for the Common Research Model

Sebastian A. Illi*, Christian Fingskes*, Thorsten Lutz†
and Ewald Krämer‡
Institute of Aerodynamics and Gas Dynamics, University of Stuttgart, Stuttgart, 70569, Germany

Downloaded by NASA Langley Research Ctr on February 7, 2014 | http://arc.aiaa.org | DOI: 10.2514/6.2013-2510

In advance of the ESWI^{RP} measurement campaign in the European Transonic Wind Tunnel in 2014, numerical simulations for NASA's Common Research Model were performed using the DLR TAU code. The presented investigations are focused on the interaction between the separated flow of the main wing with the horizontal tail plane at high Mach numbers. This phenomenon, called transonic tail buffet, poses a serious risk and therefore limits the flight envelope for commercial aircraft.

A mesh for the CRM was built including a high resolved tetrahedral block to reduce dissipative effects in the wake. A validation was conducted which shows excellent agreement to the results of the Drag Prediction Workshops. Based on lift polar simulations the buffet onset regime was defined and an inflow condition beyond this point was selected to perform an unsteady simulation. It is shown that a corner separation leads to a movement of the complex shock system on the upper surface of the main wing. Large vortices are shed which propagate downstream and massively influence the flow around the HTP followed by a high frequency response which is found in all integral coefficients.

Nomenclature

A	reference relation area $[m^2]$
b	span $[m]$
c	reference chord length $[m]$
c_D	drag coefficient $[-]$
c_{Dp}	pressure part of drag coefficient $[-]$
c_{Dv}	viscous part of drag coefficient $[-]$
c_f	skin friction coefficient $[-]$
c_L	lift coefficient $[-]$
c_p	pressure coefficient $[-]$
i_H	incidence angle of the HTP $[^\circ]$
M	Mach number $[-]$
p	pressure fluctuations $[N/m^2]$
q_∞	dynamic pressure $[N/m^2]$
Re	Reynolds number $[-]$
xyz	cartesian coordinates $[m]$
α	angle of attack $[^\circ]$
η	dimensionless span coordinate $[-]$
ν_t	eddy viscosity $[m^2/s]$

*Research Engineer, Aircraft Aerodynamics Group
†Head of Department, Aircraft Aerodynamics Group
‡Head of the Institute, Institute of Aerodynamics and Gas Dynamics

Copyright © 2013 by Sebastian Alexander Illi. Published by the American Institute of Aeronautics and Astronautics, Inc., with permission.

Downloaded by NASA Langley Research Ctr on February 7, 2014 | http://arc.aiaa.org | DOI: 10.2514/6.2013-2510

I. Introduction

Most commercial used transport and passenger aircraft are operating in transonic flight conditions. This flight regime is characterized by a supersonic area on the suction side of the wing. At its downstream position a shock system emerges which leads to a adverse pressure gradient in the boundary layer. Beyond design point conditions the boundary layer in this area may separate and lead to global flow unsteadiness. The unsteady wake propagates downstream and interacts with the empennage. Depending on the spectral content of the wake, a structural response of the horizontal or vertical tail planes can be safety critical. Therefore, an understanding of this phenomenon is of high interest for the aircraft industry.

Nowadays numerical methods are used to solve the Reynolds Averaged Navier-Stokes equations (RANS) and therefore investigate such phenomena. Lee performed numerical simulations on two-dimensional buffet and developed a theoretical buffet model which is the most popular in literature.[11] He described transonic buffet as self sustaining loop. Due to the high adverse pressure gradient in the vicinity of the shock the boundary layer separates which leads to a reduction of the effective camber of the airfoil. The shock starts to move upstream where it loses strength and the boundary layer is able to reattach followed by a shock movement in the opposite direction. At the time of boundary layer separation, pressure waves propagate from the root of the shock wave to the trailing edge. There they interact with the disturbances generated at the trailing edge. So-called Kutta-waves are generated which travel upstream.[23] Lee describes them as an energy transfer mechanism to conserve the self sustained shock movement.

An advancement of that theory gives Crouch et al.[3] who discern more complex mechanism in it. After the upstream traveling pressure waves reach the shock wave, they move about it and dissipate there slowly. On the lower side of the airfoil also pressure waves move upstream along the surface until they dissipate as well. So far it is not just a closed loop behind the shock wave but a periodically oscillating structure along the entire airfoil. It was possible to reproduce these effects[8] using the Reynolds Stress Model of Jakirlic and Hanjalic.[10] In consequence of the periodically pressure oscillations the elastic wing is going to oscillate, too. Under specific circumstances this behavior can lead to catastrophically vibrancies until structural collapse occurs. To better understand this correlation D. E. Raveh compared the buffet frequency of an rigid airfoil to the frequency of a controlled oscillating airfoil motion.[17] This study showed a direct correlation between both frequencies. It was possible to almost vanish the amplitude of the buffet if the airfoil oscillates with the same frequency.

Although these investigations lead to a better understanding of buffet on airfoils the main challenge is to understand the effects for aircraft. Past research activities were conducted for military aircraft[16] or were not focused on the wake development.[4,14,20] Therefore, the Institute of Aerodynamics and Gas Dynamics (University of Stuttgart) together with ONERA, DLR, TsAGI, VZLU, the Von Karman Institute of Fluid Dynamics and the Institute of Thermodynamics (Academy of Sciences of the Czech Republic) initiated a measurement campaign within the framework of the European project $ESWI^{RP}$ (European Strategic Wind tunnels Improved Research Potential). The main objective is a better understanding of the aerodynamics in high speed and low speed stall conditions and its influence on the wake and the empennage. The experiments will be performed in the European Transonic Wind Tunnel (ETW) on NASA's Common Research Model (CRM), which is well known from the Drag Prediction Workshops (DPW).[25]

In preparation for the measurement campaign in 2014 the Institute of Aerodynamics and Gas Dynamics performed numerical simulations using the DLR TAU code to identify critical inflow conditions for the CRM. First of all the numerical method in combination with a high resolved mesh is validated on results of the 4^{th} and 5^{th} DPW. After determining the stall conditions for High Speed Stall with steady-state RANS lift polar simulations, a URANS simulation at a critical angle of attack is performed which allows characterizing the main features of transonic tail buffet and helps identifying the locations for the Particle Image Velocimetry (PIV) measurements in the wake and their temporal and spatial resolution.

II. Numerical Setup

A. DLR TAU Code

The DLR TAU Code is a German research CFD solver which is based on a unstructured finite volume scheme.[7] The code is developed by the German Aerospace Center (DLR) and used by several German universities and the aircraft industry. A cell vertex grid metric is implemented for structured and unstructured cell types. For the following unsteady CFD simulations the LUSGS scheme with dual time stepping was used.

In every physical time step 120 inner iterations were needed to assure convergence of the global coefficients and reduce the residuals to acceptable values. The spatial discretization of the fluxes is performed using a central scheme where matrix dissipation was applied to the convective fluxes. A 3v multigrid cycle is used to improve the convergence rate during the inner iterations.

For turbulence treatment the Spalart-Allmaras model was used in the following investigations. This turbulence model was mainly used in the Drag Prediction Workshops and is well known due to its simplicity and robust behavior. Only an additional transport equation for $\tilde{\nu}$, a derivative of the turbulent viscosity, is solved.[22]

B. Geometry

The geometry of the Common Research Model (CRM) is based on the description of Vassberg et al.[24] The design point was defined for a Reynolds number of $Re = 40{\cdot}10^6$ at a transonic Mach number of $M = 0.85$ and a lift coefficient of $c_L = 0.5$. For the full scale model a reference relation area of $A = 383.69m^2$ with a reference chord length of $c = 7.005m$ was calculated. The geometry was deformed for a 1g loading case as it was already done in the Drag Prediction Workshops. Due to symmetric inflow conditions for the current studies only a semi-model of the CRM was used for the simulations to reduce computational cost.

The model including the horizontal tail planes was used to investigate the conditions on the empennage. The incident angle of the horizontal tail plane is set to $i_H = 0°$. All relevant data are summarized in Fig. 1.

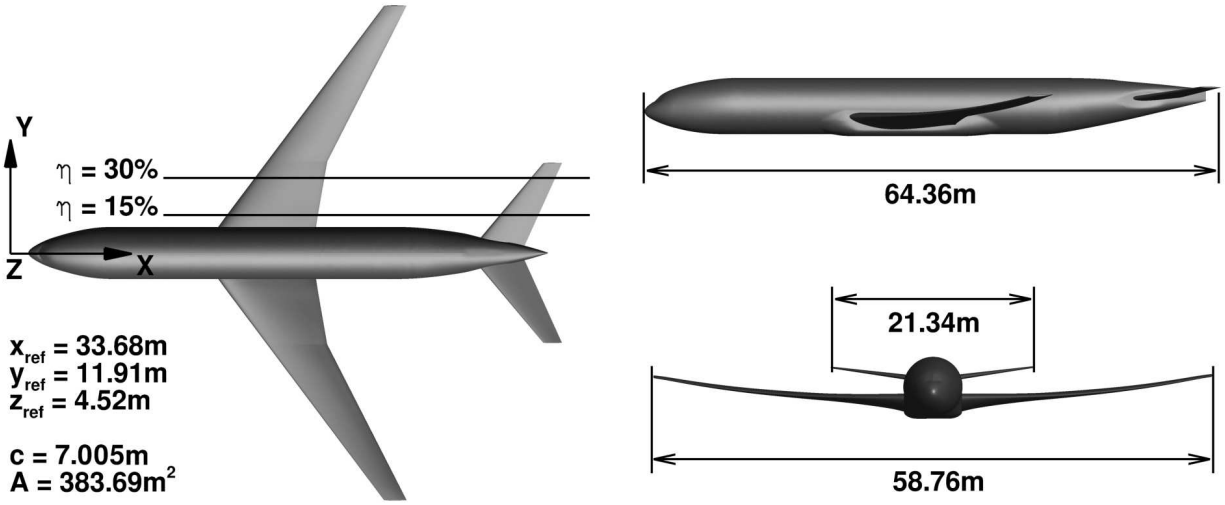


Figure 1. Wing-Body-Tail Configuration of the NASA Common Research Model

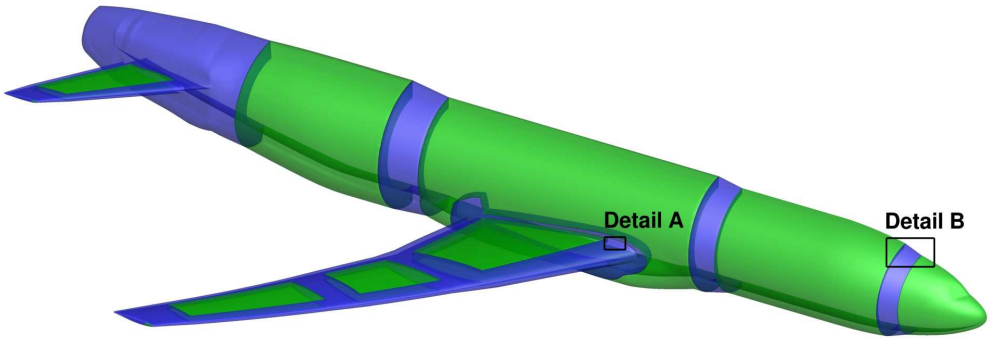
C. Grid Generation

For the grid generation the commercial software Gridgen^{TM} of Pointwise Inc. was used. On the surface prism and hexahedra blocks were extruded to resolve the boundary layer properly. Therefore, the dimensionless wall distance y^+ was estimated for the given Reynolds number with the equations for the flat plate case. For the boundary layer height a safety factor of 2 was added concerning adverse pressure gradient of the wing. Fig. 2(a) shows the distribution of structured (blue) and unstructured (green) blocks. The unstructured prism blocks are used in the main areas of the boundary layer. Due to boundary layer growth along the stream-wise coordinate, it was necessary to divide fuselage, wing, and tail into certain segments. In each segment the height of the boundary layer has a constant value. The junctions between them equate the relative height to each other like it is shown in Fig. 2(b).

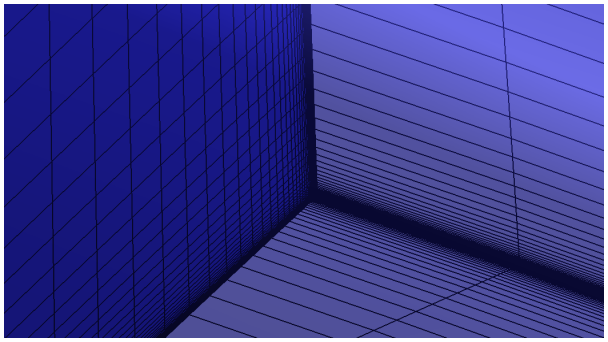
The most sophisticated part of meshing is the section where wing and tail are connected to the fuselage. There two different boundary layers encounter each other. In consequence the interaction in the flow generates vortices, which may lead to prematurely detachment in this section. As the study of Sclafani et al.[21] shows, different varieties of concave corner meshing have a strong influence on the solution. Due to good results

Downloaded by NASA Langley Research Ctr on February 7, 2014 | http://arc.aiaa.org | DOI: 10.2514/6.2013-2510

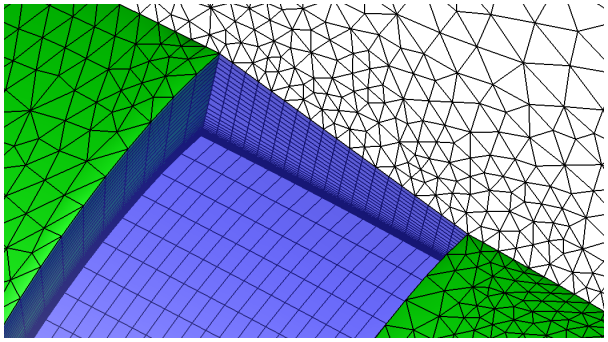
Downloaded by NASA Langley Research Ctr on February 7, 2014 | http://arc.aiaa.org | DOI: 10.2514/6.2013-2510



(a) boundary layer with hexahedra (blue) and prisms (green)



(b) Detail A: wing fuselage intersection



(c) Detail B: junction between two prism blocks

Figure 2. IAG Gridgen Netz des CRM

with the *Patch Grid*, this kind of meshing was used for the IAG mesh illustrated in Fig. 2(b). As it is shown in the results, the vortex at the trailing edge has a big influence on the buffet phenomenon as well.

The boundary layer mesh was embedded into a tetrahedral mesh.High resolved areas were defined in the area around the expected shock system on the upper surface of the wing and in the wake. A farfield boundary condition was set in a radius of 250c. The volume in-between was solved with the tetrahedral algorithm of Gridgen^{TM}.

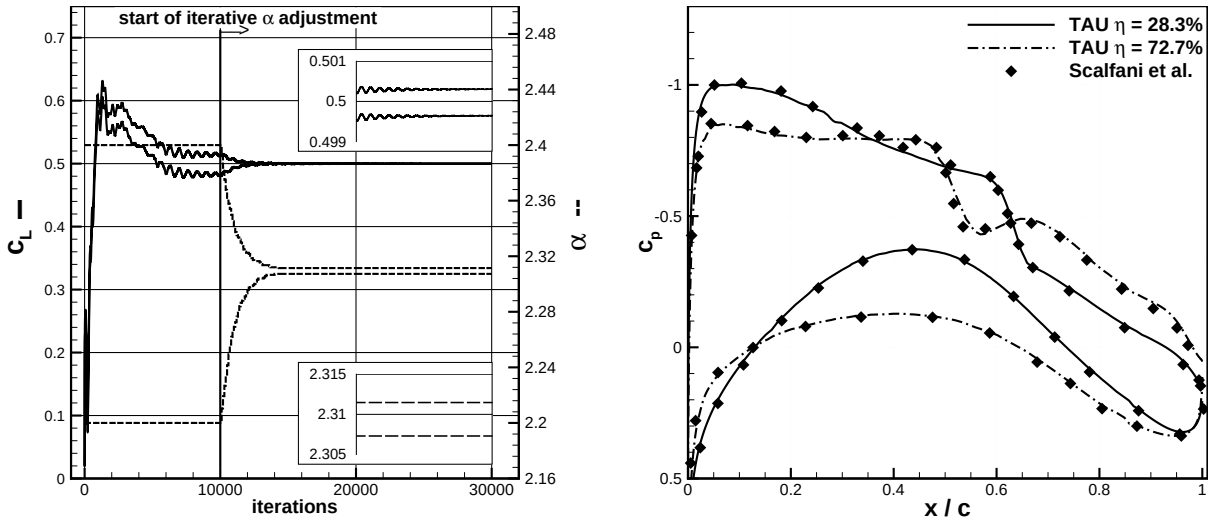
Comparing the size of the IAG mesh with its 14.5M points to the DPW meshes it is located in the medium range. Altogether it consists of 5.0M prism, 7.4M hexahedral and 20.5 tetrahedral elements.

III. Results

A. Validation

The performed TAU simulations were validated on the cases of the Drag Prediction workshop according to Morrison[15] and on the experimental results of Rivers and Dittberner.[18]

First of all *Morrison's case 1* is simulated on the newly generated mesh. The Reynolds number is set to $Re = 5{\cdot}10^6$ and the Mach number to $M = 0.85$. Fig. 3(a) shows the convergence history for the angle of attack α and the lift coefficient c_L. An iterative scheme was used which varies α to achieve $c_L = 0.5$ and is activated after 10000 iterations. Two simulations were performed starting with an angle of attack above and below the expected angle of the results shown by Morrsion.[15] The detail on the top of Fig. 3(a) shows that a convergence below the indicated accuracy of $c_L = 0.5 \pm 0.001$ was achieved for both simulations. The angle



(a) Convergence histories

(b) Comparisson to Sclafani et al.[21]

Figure 3. Validation Case 1 $Re = 5{\cdot}10^6$, $M = 0.85$, $c_L = 0.5$

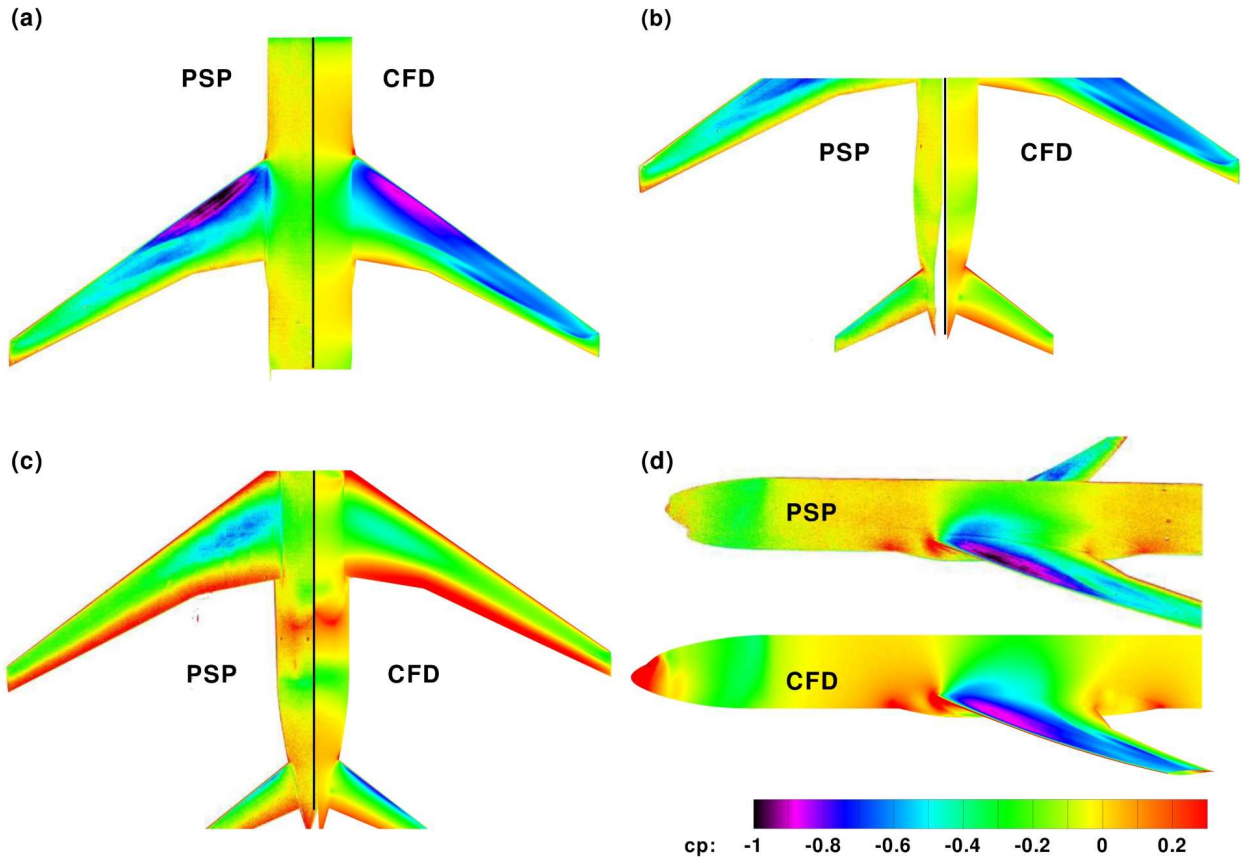


Figure 4. Comparisson of TAU CFD simulations to PSP data of James H. Bell,[2] $Re = 5 \cdot 10^6$, $M = 0.85$, $\alpha = 1.5°$, (a) left wing and fuselage upper surface, (b) upper horizontal tail and aft fuselage, (c) lower surface of the wing, aft fuselage and horizontal tail, (d) left wing root obliquely

Downloaded by NASA Langley Research Ctr on February 7, 2014 | http://arc.aiaa.org | DOI: 10.2514/6.2013-2510

of attack α is located around 2.31°. A comparison in Table 1 to the grid convergence study core medians of the 4th Drag Prediction Workshop[15] shows that this value is within the bounds of the given standard deviations. The values listed for the drag counts are also in good agreement compared to the participant results of the DPW.

Sclafani et al.[21] investigated the influence of the numerical scheme and the mesh resolution and published pressure distributions for two y-planes at the dimensionless span coordinate $\eta = 28.3\%$ and $\eta = 72.7\%$. Their results on the fine mesh are compared to the TAU results in Fig. 3(b). In both planes the pressure distributions look quite identical. Only the shock position in the outer section $\eta = 72.7\%$ is slightly shifted downstream for the TAU results.

Bell published measurement data using pressure sensitive paint (PSP) for almost the whole surface of the CRM at a Reynolds number of $Re = 5{\cdot}10^6$, a Mach number of $M = 0.85$ and $\alpha = 1.5°$.[2] The TAU simulations compared to these results in Fig. 4 show all the expected properties of the flow. In Fig. 4(a) the upper surface of the wing and the fuselage is illustrated. A strong suction peak is present around the leading edge of the inner section of the wing followed by a shock. On the outer segment also a low pressure area is located up to the mid-chord of the wing, followed by a compression and an instantly appearing low pressure area which can also be found in the PSP results. Fig. 4(b) highlights the upper surface of the horizontal tail plane and the aft fuselage. In Fig. 4(c) the lower surface of the wing and the horizontal tail plane are shown. In both figures the pressure distributions of the numerical simulation are in excellent agreement with the PSP results. An oblique view of the left side of the CRM is finally shown in Fig. 4(d). The low pressure area after the cockpit as well as the stagnation points at the beginning and tail of the belly fairing are well represented.

However, the pressure values at the suction side of the wing are a little underestimated at the inner and overestimated at the outer section of the wing. An investigation of this topic was published by Rivers et al.[19] They made the stronger twist of the wings in the wind tunnel experiments responsible for the discrepancy in the pressure distributions.

Because the aim of the simulations is to define buffet conditions for the ESWI^{RP} case at an increased Reynolds number of $Re = 30{\cdot}10^6$, further comparisons to Sclafani et al.[21] were carried out. Table 1 shows the results at Reynolds numbers of $Re = 20{\cdot}10^6$ and $30{\cdot}10^6$. Like it is expected a higher Reynolds number results in a thinner boundary layer, leading to an enhanced lift coefficient for the same angle of attack. Therefore, the angle of attack for constant $c_L = 0.5$ is reduced compared to the $Re = 5{\cdot}10^6$ case which also results in a reduction of the drag coefficient c_D. The TAU results at $Re = 20{\cdot}10^6$ are in good agreement ($\pm$ 4 drag counts) with the results of Sclafani et al. and the values for the $Re = 30{\cdot}10^6$ case seem reasonable.

Wing-Body-Tail Configuration (i_H=0°), M = 0.85, $c_L = 0.50$					
Case	Re [-]	α [°]	c_D counts [-]	c_{Dp} counts [-]	c_{Dv} counts [-]
4^{th} DPW coarse[15]	$5 \cdot 10^6$	2.340 ± 0.085	279 ± 8.8	158 ± 8.8	124 ± 5.7
4^{th} DPW medium[15]	$5 \cdot 10^6$	2.324 ± 0.084	274 ± 6.1	151 ± 4.8	125 ± 4.5
4^{th} DPW fine[15]	$5 \cdot 10^6$	2.343 ± 0.24	272 ± 6.1	148 ± 4.6	125 ± 3.9
Sclafani et al[21]	$5 \cdot 10^6$	2.364	270.6	-	-
IAG Gridgen Mesh	$5 \cdot 10^6$	2.307	277.5	150.0	127.5
IAG Gridgen Mesh	$5 \cdot 10^6$	2.312	277.8	150.3	127.5
Sclafani et al[21]	$20 \cdot 10^6$	2.183	240.4	-	-
IAG Gridgen Mesh	$20 \cdot 10^6$	2.119	244.7	138.4	106.2
IAG Gridgen Mesh	$20 \cdot 10^6$	2.121	244.8	138.6	106.2
IAG Gridgen Mesh	$30 \cdot 10^6$	2.072	236.8	135.8	101.0
IAG Gridgen Mesh	$30 \cdot 10^6$	2.075	237.1	136.1	101.0

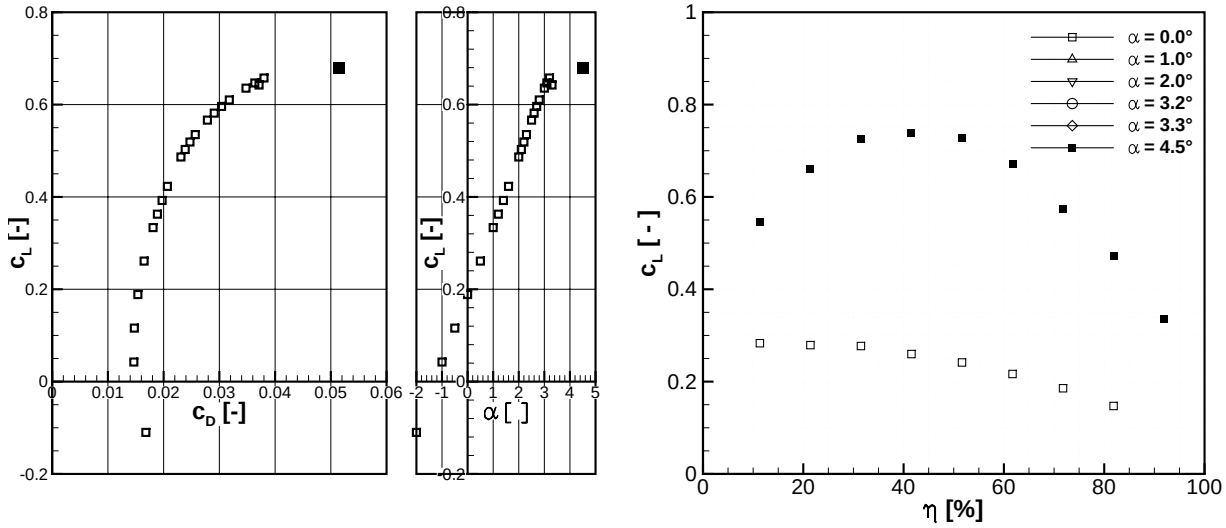
Table 1. Comparisson of IAG results to the Drag Prediction Workshops

Downloaded by NASA Langley Research Ctr on February 7, 2014 | http://arc.aiaa.org | DOI: 10.2514/6.2013-2510

B. Determination of Buffet-Onset conditions

In preparation of the ESWI^{RP} project the conditions for transonic buffet had to be defined. Therefore, in a first place RANS simulations at the test conditions of $Re = 30 \cdot 10^6$ and $M = 0.85$ were performed to define the linear regime of the lift polar. In Fig. 5(a) the results of a α-sweep from α = -2° to $\alpha = 3.3°$ are shown with a decreased $\Delta\alpha$ for higher angles of attack. The lift polar presents a linear behavior up to $\alpha \approx 2.8°$. Starting from that position the gradient $\partial c_L/\partial\alpha$ is slightly decreased. The RANS result gives a maximum lift of $c_L = 0.658$ for $\alpha = 3.2°$. For further increase of the angle of attack the lift is reduced due to separation effects on the upper surface of the main wing.

This behavior was further investigated in Fig. 5(b). Here the lift coefficient in slices parallel to the y-plane as a function of the dimensionless span coordinate η is shown. An elliptic shape can be seen like it is expected for wings of modern aircraft. An increase of the angle of attack leads to higher c_L values all over the span up to $\alpha = 3.2°$. At $\alpha = 3.3°$ a drop of lift in the area of the wing fuselage intersection is noticed due to a corner separation beginning at the trailing edge. Beyond this point the convergence rates of the residuals are reduced significantly and the integral coefficients do not converge to steady state.



(a) Drag and lift polars

(b) Lift distribution on the spanwise coordinate η

Figure 5. Alpha sweep for $Re = 30{\cdot}10^6$, $M = 0.85$ using RANS (hollow symbols), URANS (filled symbols)

The drag coefficient c_D in Fig. 5(a) shows a minimum for $c_L \approx 0$. Outgoing from that position the aerodynamic drag rises with increasing lift. The lift-to-drag ratio shows a maximum for $c_L = 0.5$ which is known to be the design point of the Common Research Model. Beyond this point the shock system on the upper side of the wing becomes stronger, leading to transonic drag rise and finally to buffet-onset. Balakrishna and Acheson[1] evaluated the experimental results performed in the Langley National Transonic Facility and the Ames 11-foot Transonic Wind Tunnel. They used the so-called *Buffet Intensity parameter*

$$c_B(\alpha) = \frac{\int_0^{fMAX} S_a(f)\,df}{\int_0^{fMAX} S_0(f)\,df}$$

based on the CRM wing-root bending moment energy to determine the onset conditions. For $Re = 30 \cdot 10^6$ and $M = 0.85$ this parameter starts to grow for $\alpha \approx 3°$ denoting a beginning separation. This result is in good agreement with the here presented RANS polar simulations. Balakrishna and Acheson show that the Buffet Intensity parameter reaches high values of $c_B > 1.5$ at $\alpha \approx 4.5°$. At this position also the RMS strain starts to rise significantly indicating strong unsteady effects.

Due to the good agreement of the TAU RANS simulations to the experimental data of Balakrishna and Acheson and their evaluation of c_B, the unsteady simulation for transonic buffet is performed at an angle of attack of $\alpha = 4.5°$.

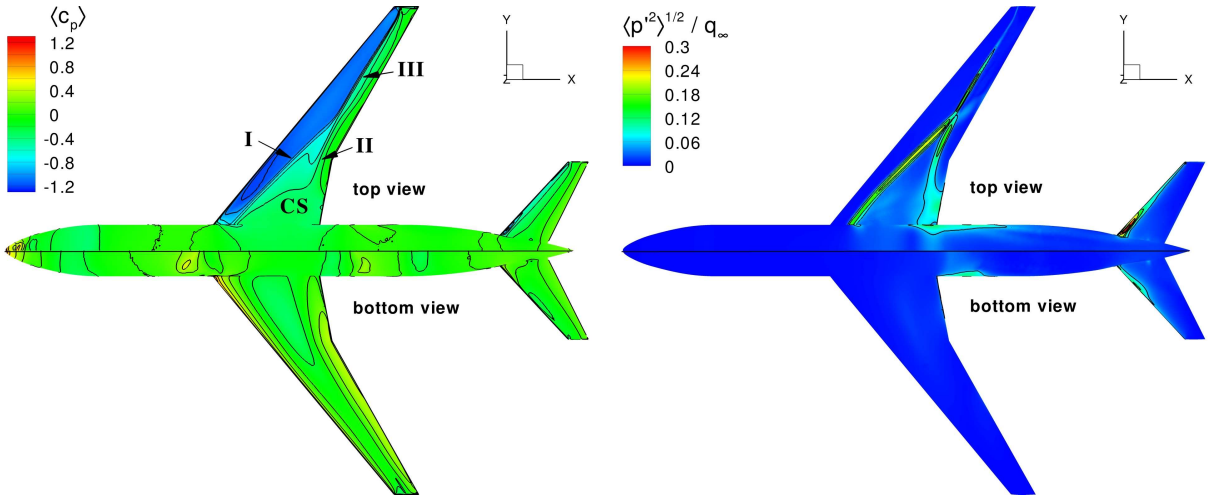
Downloaded by NASA Langley Research Ctr on February 7, 2014 | http://arc.aiaa.org | DOI: 10.2514/6.2013-2510

C. Unsteady Buffet Simulations

At the previously defined conditions unsteady RANS (URANS) simulations were performed on the grid described in section C. An implicit dual time stepping scheme was used where the convective time ΔT is based on the characteristic length c and the free stream velocity U_∞.

$$\Delta T = c/U_\infty$$

Every convective time is resolved by 150 time steps and every time step converges within 120 inner iterations. For the presented results the means, RMS-values and the spectra were evaluated over 65 convective times resulting in 1.2 million inner iterations. Therefore, the mesh was split into 512 domains and the simulations were performed on the CRAY XE 6 *Hermit* at the HLRS in Stuttgart. For up to 10000 points / domain TAU performs excellent on such systems like it was shown by the authors before.[9]



(a) Mean pressure distribution

(b) Variances of pressure

Figure 6. Case for transonic buffet $Re = 30{\cdot}10^6$, $M = 0.85$, $\alpha = 4.5°$

First of all the time averages of the integral force coefficients c_L and c_D are compared to the results of the steady RANS simulations in Fig. 5(a). The average lift coefficient is slightly increased compared to the steady result for maximum lift at $\alpha = 3.2°$. The averaged value for c_D seems to be in good agreement with the shape of the drag polar and shows a strong increase in drag at these conditions. In Fig. 5(b) also the averaged values for the c_L (η)-function were included. The distribution shows a strong decline in lift around the wing fuselage intersection but increased values at the outer span coordinates.

Fig. 6(a) shows the averaged pressure distribution on the surface of the Common Research Model from top and bottom view. It can be seen that at these conditions very low pressure levels are present around the leading edge of the upper surface indicating high Mach numbers in these areas. The supersonic areas are finished by a complex shock system which is divided into three main areas. The first shock (I) starts at the fuselage at approximately 20% of the local chord length and extends in a deflection angle of 50° to $\eta =$ 53%. A second weaker shock (II) is located right behind the main shock system in an angle accordingly to the sweep angle of the trailing edge. This shock is pushed away from the fuselage by the corner separation (CS) and encounters shock (I) at $\eta = 53\%$. There they merge into shock (III) which extends with the sweep angle of the outer segment's trailing edge right to the wing tip.

The unsteadiness of the shock system is indicated in Fig. 6(b). There the RMS-values of the pressure coefficient are shown. A periodically movement of the shocks is forced by the corner separation which leads to high RMS-values due to the large pressure gradients in this area. The whole shock system is involved in the unsteady shock buffet and seems to shift up to 10% respectively to the local chord length. Besides the shock system in the vicinity of the corner separation at the trailing edge high RMS-values can be recognized. This heavily unsteady area extends far downstream and its footprint can be found also on the surface of the fuselage. Because the corner separation seems to play a major role in the shock buffet of the CRM it should be mentioned that eddy viscosity models tend to overestimate these bubbles. Investigations on this matter

Downloaded by NASA Langley Research Ctr on February 7, 2014 | http://arc.aiaa.org | DOI: 10.2514/6.2013-2510

have been performed e.g. by Gand et al.[6] and also have been discussed in the 5^{th} DPW.[12] Nevertheless the prediction presented here can be classified as a conservative estimation while for RSM or (hybrid) LES turbulence modeling a weaker corner separation is expected.

Accordingly to the chosen inflow conditions no high RMS-values are expected for undisturbed flow at the horizontal tail plane. However, Fig. 6(b) shows strongly increased RMS-levels around the leading edge of the HTP. The only explanation for this behavior is located in the propagation of the turbulent wake of the main wing to the HTP. The turbulent structures induce velocity fluctuations and have a significant influence on the pressure distribution. Fig. 7 shows vortices using iso-surfaces of the λ_2-criterion for λ_2 = -1. To visualize the modeled turbulent content the eddy-viscosity ν_t is also drawn and the separated areas on the CRM can be identified by surface streamlines based on the skin friction vector $\vec{c_f}$.

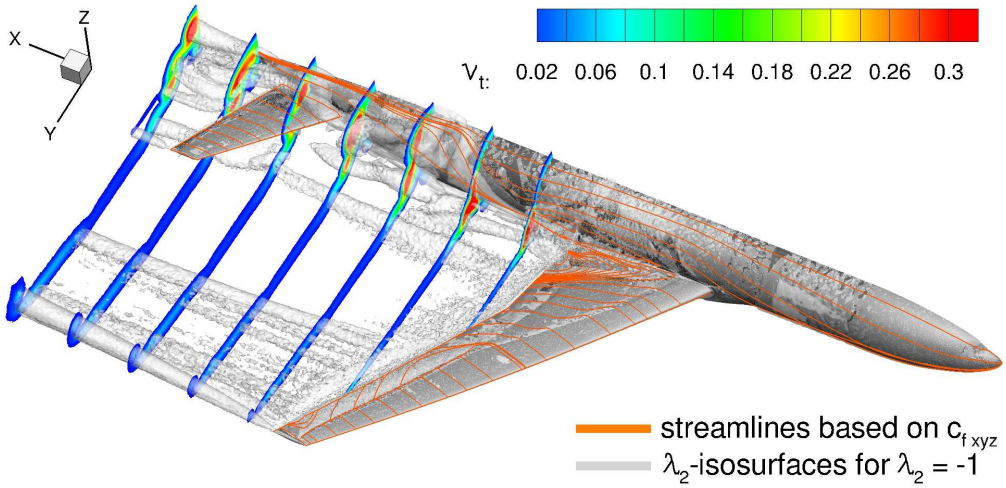


Figure 7. Visualization of the flow field $Re = 30{\cdot}10^6$, $M = 0.85$, $\alpha = 4.5^\circ$

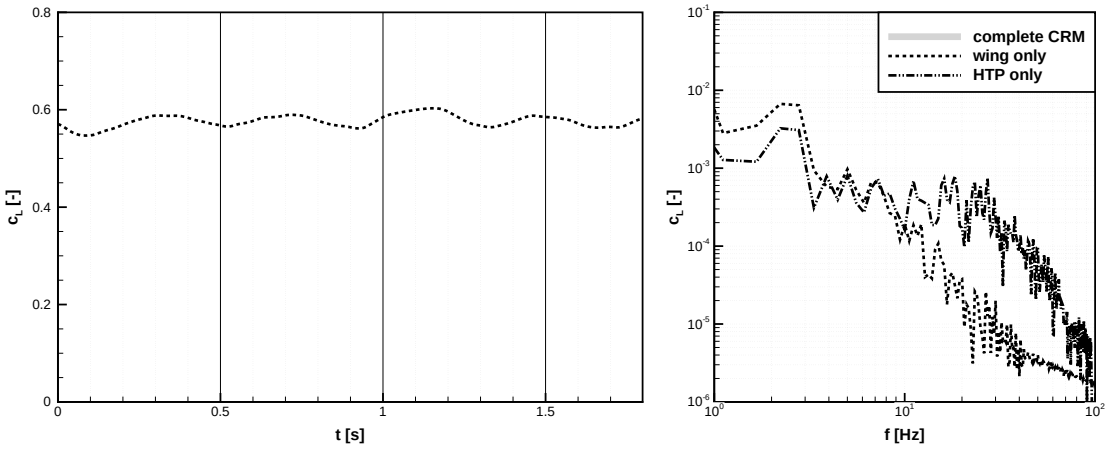
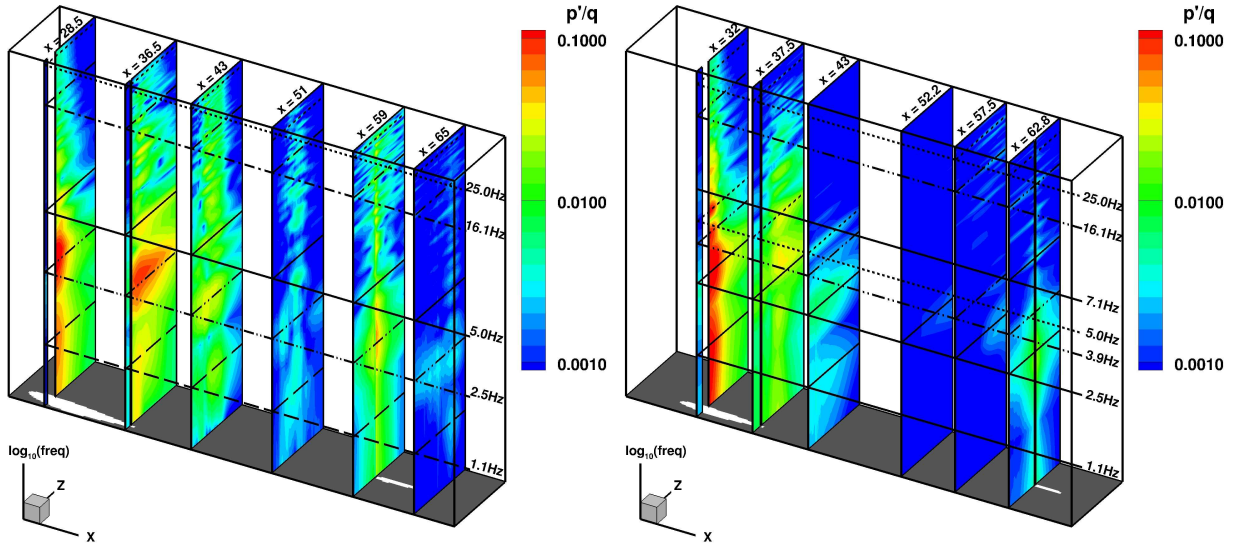


Figure 8. Temporal development of the lift coefficient (left) and its spectra (right)

The conical shaped tip vortex of the main wing can be seen clearly as well as the tip vortex of the HTP. From the corner separation, which was already mentioned in Fig. 6(a), a huge vortex system is established which is identified to be the main reason for the disturbed pressure distribution on the HTP. The whole region around the body shows high levels of ν_t indicating strong turbulent movement. Also the separated area behind shock (III) has an influence on the wake. But there the levels of eddy viscosity are an order of magnitude lower and the positions of the vortices do not allow a direct interaction with the HTP.

In Fig. 8 the lift coefficient was split into the single parts of the wing and the horizontal tail plane. At the wing a large harmonic oscillation can be found. The spectrum on the right-hand side shows a peak at around $f = 2.5$ Hz. This frequency correlates with the pulsating corner separation and the induced movement of

Downloaded by NASA Langley Research Ctr on February 7, 2014 | http://arc.aiaa.org | DOI: 10.2514/6.2013-2510



(a) $\eta = y/(b/2) = 15\%$ (b) $\eta = y/(b/2) = 30\%$

Figure 9. Spectral development of the pressure fluctations between the wing and the horizontal tail plane

the shock system on the upper surface of the wing. The same plateau exists in the spectrum of the HTP but there a plateau with high amplitudes can also be found between $f = 10...30$ Hz.

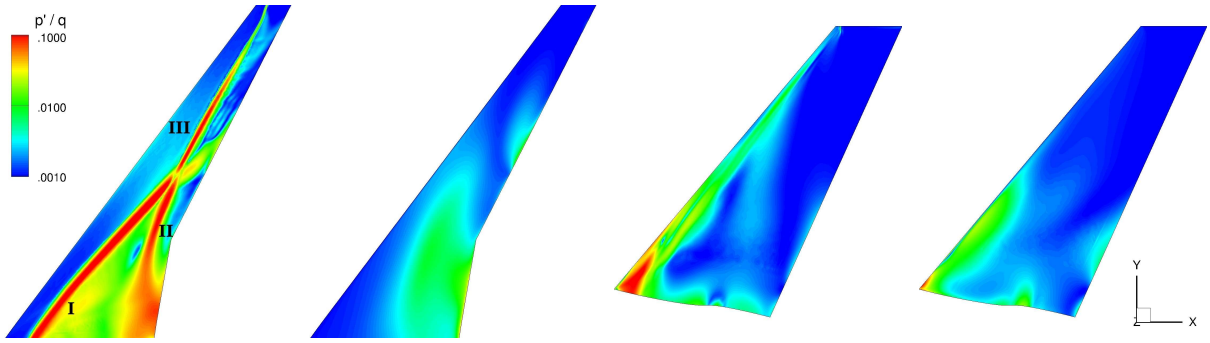
For Fig. 9(a) and 9(b) the pressure p was monitored in the whole flow domain and normalized with the dynamic pressure of the freestream q. After averaging a Fourier transformation was applied to the signals in two xz-planes at spanwise positions $\eta = 15\%$ and $\eta = 30\%$. The location of the two slices are also seen in Fig. 1.

Lines parallel to the z-coordinate have been extracted at six different positions. On the bottom plane of the figures the shape of the wing and the HTP is drawn. Perpendicular to this plane the logarithmic frequency is plotted ranging from 0.5 to 27Hz. The first slice on the left is located in the vicinity of the moving shock on the suction side of the main wing. Two plateaus with high pressure amplitudes are found with peaks around $f = 1.1$Hz and around $f = 2.5$ Hz.

A visualization of the pressure coefficient system reveals that the main movement frequency of the shock is located around $f = 2.5$ Hz and that the whole wake is meandering around that frequency. For $\eta = 15\%$ this mode is found in the whole wake and amplified significantly around the leading edge of the HTP. The mode shape has been analyzed on the surfaces of the wing and the HTP in Figs. 10(a) to 10(d). Around shock (I) on the suction side of the wing the strongest shock movement is seen but the 2.5 Hz frequency is present for all shock locations (I-III). The influence of the oscillating flow field can also be found on the pressure side of the wing in Fig. 10(b) where it extends from the trailing edge in two centers located at $\eta = 30\%$ and $\eta = 60\%$.

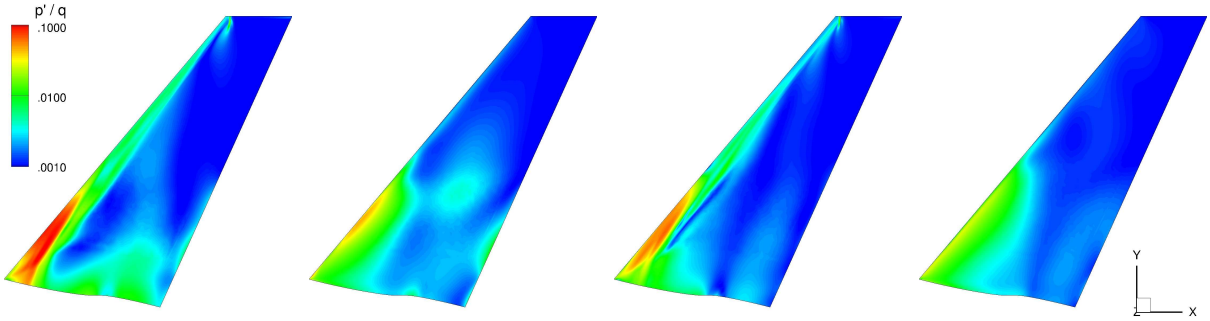
Around the HTP the 2.5 Hz mode is found especially in the vicinity of the leading edge. The strongest pressure fluctuations are located around the area of the HTP fuselage intersection. This area is directly influenced by the vortex shedding of the corner separation. The 2.5 Hz are related to a big vortex system which is produced every time shock (I) starts to move upstream. These fluctuations are in the same order of magnitude as on the wing around the shock positions (I-III) and dominate the oscillating lift coefficient of the HTP. However, strong modes also can be found on higher frequencies. Figs. 9(a) and 9(b) reveal, that modes between 10 and 30 Hz are amplified significantly near the leading edge of the HTP. This frequency range is equivalent to the continuously shed vortices of the corner separation. Two of these high frequent modes are plotted in Figs. 11(a) to 11(d), namely the 16.1 Hz and 25.0 Hz modes. The strongest amplitudes are also found here near the fuselage intersection where the vortices impinge directly on the HTP. The tip region of the HTP where all modes also can be found at smaller amplitudes is indirectly influenced by these vortices and the meandering of the wake behind the wing.

Downloaded by NASA Langley Research Ctr on February 7, 2014 | http://arc.aiaa.org | DOI: 10.2514/6.2013-2510



(a) upper side wing (b) lower side wing (c) upper side HTP (d) lower side HTP

Figure 10. 2.5 Hz pressure modes on the surfaces of the wing and the HTP



(a) upper side HTP, 16.1 Hz (b) lower side HTP, 16.1 Hz (c) upper side HTP, 25.0 Hz (d) lower side HTP, 25.0 Hz

Figure 11. higher frequent pressure modes on the surfaces of the HTP

IV. Conclusions

The aim of the current investigations is to define the inflow conditions for the measurement campaign at the Common Research Model in the ETW in 2014. Detailed numerical simulations were performed aiming at the conditions of transonic tail buffet. Therefore, a new mesh for the increased Reynolds number of $Re = 30{\cdot}10^6$ was built including a high resolved tetrahedral block between the main wing and the HTP to improve the resolution of the wake.

The presented validation is in good agreement with the publications of the Drag Prediction Workshops[15] and is even comparable to PIV measurements by James H. Bell.[2] The α-sweep at $Re = 30{\cdot}10^6$ shows a linear behavior up to an angle of attack of $\alpha = 3.2°$. Beyond that position the Spalart Allmaras turbulence model shows a corner separation at the intersection of the main wing and fuselage. This leads to non-linear effects and unsteady behavior of the flow which is in good agreement with the dynamic data analysis of the CRM by Balakrishna and Acheson.[1]

Based on these results the angle of attack for the URANS simulation was set to $\alpha = 4.5°$ at a Mach number of $M = 0.85$. The simulation shows strong unsteady effects on the suction side of the wing. The shock boundary layer interaction near the fuselage leads to a corner separation, which is followed by a periodical movement of the complete shock system on the wing. The HTP is massively influenced by these unsteady effects resulting in a separation around the leading edge and a high frequency response.

Because the main effects of transonic tail buffet seem to take place in the wake close to the fuselage, the PIV measurements during the $ESWI^{RP}$ campaign will be performed in xz-planes at $\eta = 15\%$ in three different positions. The first one is located close to the trailing edge of the main wing, the second one close to the leading edge of the HTP and the third one right in the middle of the wake. Furthermore, the temporal and spatial resolution for the PIV was chosen based on the here provided pressure spectra in the wake. A detailed description of the experimental settings was published by Lutz et al.[13]

Downloaded by NASA Langley Research Ctr on February 7, 2014 | http://arc.aiaa.org | DOI: 10.2514/6.2013-2510

Acknowledgments

The authors gratefully acknowledge the support and the computational resources which were provided by the High Performance Computing Center Stuttgart (HLRS). The simulations were performed on the CRAY XE 6 (Hermit) which is funded by Federal Ministry of Education and Research and the Ministry of Higher Education, Research and Arts Baden-Württemberg.

References

[1]Balakrishna, S., and Acheson, M., *Analysis of NASA Common Research Model Dynamic Data*, 49th AIAA Aerospace Sciences Meeting including the New Horizons Forum and Aerospace Exposition, 2011-1127, AIAA, 2011.

[2]Bell, J. H., *Pressure-Sensitive Paint Measurements on the NASA Common Research Model in the NASA 11-ft Transonic Wind Tunnel*, 49th AIAA Aerospace Sciences Meeting including the New Horizons Forum and Aerospace Exposition, 2011-1128, AIAA, 2011.

[3]Crouch, J. D., Garbaruk A., Magidov, D., and Travin, A., *Origin and structure of transonic Buffet on airfoils*, 5th AIAA Theoretical Fluid Mechanics Conference, 2008-4233, AIAA, 2008.

[4]Dandois, J., Dandois, J., Brunet, V., Molton, P., Abart, J., and Lepage, A., *Buffet Control by Means of Mechanical and Fluidic Vortex Generators*, 5th Flow Control Conference, 2010-4975, AIAA, 2010.

[5]U. Fey et al., *Transition Detection by Temperature Sensitive Paint at Cryogenic Temperatures in the European Transonic Wind Tunnel (ETW)*, 20th International Congress on Instrumentation in Aerospace Simulation Facilities, 2003, pp. 77-88.

[6]F. Gand and S. Deck V. Brunet and P. Sagaut, *Flow dynamics past a simplified wing body junction*, Phyics of Fluids, Vol. 22, 2010, 11511.

[7]Gerhold, T., *Overview of the Hybrid RANS Code TAU*, Notes on Numerical Fluid Mechanics and Multidisciplinary Design, Vol. 89, edited by N. Kroll and J. K. Fassbender, 2005, pp. 81-92.

[8]Illi, S. A., Lutz, Th., and Krämer, E., *On the capability of unsteady RANS to predict transonic buffet*, 3^{rd} Joint Symposium of DFG FOR 1066 and DLR-Airbus $C^2A^2S^2E$: "Simulation of Wing and Nacelle Stall", 2012.

[9]Illi, S. A., Lutz, Th., and Krämer, E., *Transonic Tail Buffet Simulations on the ATRA Research Aircraft*, Notes on Numerical Fluid Mechanics and Multidisciplinary Design, Springer, 2013. (to be published)

[10]Jakirlic, S., and Hanjalic, K., *A new approach to modelling near-wall turbulence energy and stress dissipation*, Journal of Fluid Mechanics, Vol. 459, 2002, pp. 139-166.

[11]Lee, B. H. K., *Self-sustained shock oscillations on airfoils at transonic speeds*, Progress in Aerospace Sciences, Vol. 37, 2001, pp. 147-196.

[12]Levy, D. W. et al., *Summary of Data from the Fifth AIAA CFD Drag Prediction Workshop*, 51st AIAA Aerospace Sciences Meeting, 2013-0046, AIAA, 2013.

[13]Lutz, Th. et al., *Going for Experimental and Numerical Unsteady Wake Analysis Combined with Wall Interfernece Assessment by Using the NASA CRM in the ETW*, 51st AIAA Aerospace Sciences Meeting, Grapevine, TX, January 7th - 11th, 2013

[14]Molton, P., Bur, R., Lepage, A., Brunet V., and Dandois J., *Control of Buffet Phenomenon on a Transonic Swept Wing*, 40th Fluid Dynamics Conference and Exhibit, 2010-4595, AIAA, 2010.

[15]Morrison, J., *Statistical Analysis of CFD Solutions from the Fourth AIAA Drag Prediction Workshop*, 28th AIAA Applied Aerodynamics Conference, 2010-4673, AIAA, 2010.

[16]Morton, S. A., Cummings, R. M., and Kholodar, D. B., *High Resolution Turbulence Treatment of F/A-18 Tail Buffet*, Journal of Aircraft, Vol. 44, 2007, pp. 1769-1775.

[17]Raveh, D. E., *Numerical Study of an Oscillating Airfoil in Transonic Buffeting Flows*, AIAA Journal, Vol. 47, No. 3, 2009, pp. 505-515.

[18]Rivers, M. B., and Dittberner, A., *Experimental Investigations of the NASA Common Research Model*, 28th AIAA Applied Aerodynamics Conference, 2010-4218, AIAA, 2010.

[19]Rivers, M. B., and Dittberner, A., *Further Investigation of the Support System Effects and Wing Twist on the NASA Common Research Model*, 30th AIAA Applied Aerodynamics Conference, 2012-3209, AIAA, 2012.

[20]Rumsey, C. L. et al., *CFD Sensitivity Analysis of a Modern Civil Transport Near Buffet-Onset Conditions* NASA, TM-2001-211263, 2001.

[21]Sclafani, A. J., DeHaan, M., Vassberg, J., Rumsey, C. L., and Pulliam, T., *Drag Prediction for the NASA CRM Wing-Body-Tail using CFL3D and Overflow on an Overset Mesh*, 28th AIAA Applied Aerodynamics Conference, 2010-4219, AIAA, 2010.

[22]Spalart, P. R., and Allmaras, S. R, *A One-Equation Turbulence Model for Aerodynamic Flows*, AIAA, Vol. 439, 1992.

[23]Tijdeman, H., *Investigations of the transonic flow around oscillating airfoils*, Ph.D. Dissertation, TU Delft, 1977.

[24]Vassberg, J., and Dehaan, M. A., *Development of a Common Research Model for Applied CFD Validation Studies*, 26th AIAA Applied Aerodynamics Conference, 2008-6919, AIAA, 2008.

[25]Vassberg, J. et al., *Summary of the Fourth AIAA CFD Drag Prediction Workshop*, 28th AIAA Applied Aerodynamics Conference, 2010-4547, AIAA, 2010.

Downloaded by NASA Langley Research Ctr on February 7, 2014 | http://arc.aiaa.org | DOI: 10.2514/6.2013-2510